

A SPDC-BASED SOURCE OF ENTANGLED PHOTONS AND ITS CHARACTERIZATION

S. Magnitskiy,^{1*} D. Frolovstev,¹ V. Firsov,¹ P. Gostev,¹ I. Protsenko,^{2,3} and M. Saygin^{1,2,3}

¹*Faculty of Physics and the International Laser Center
Lomonosov Moscow State University
Leninskie Gory, Moscow 119992, Russia*

²*Laboratory of Optoelectronic Devices Ltd.
First Magistralnaya Street 13, bld. 7, Moscow 123007, Russia*

³*Lebedev Physical Institute, Russian Academy of Sciences
Leninskii Prospect 53, Moscow 119991, Russia*

*Corresponding author e-mail: sergeymagnitskiy@gmail.com

Abstract

We present a short review of development and applications of single and biphoton sources. The main emphasis is on spontaneous parametric down-conversion (SPDC) sources capable of producing time-correlated photon pairs. We also present a SPDC source of photon pairs at 1,064 nm pumped by a cw 532 nm laser. We consider the fundamental principles of quantum tomography and present results of characterization (entanglement and purity) of biphoton quantum states produced by this source. Additionally, we discuss some aspects of quantum entanglement suppression caused by the Migdall effect in a double-crystal scheme.

Keywords: spontaneous parametric down-conversion, polarization-entangled states, correlated photons, quantum tomography.

1. Introduction

Optics and especially quantum optics play an important role in modern quantum technologies due to the unique features of the optical fields. The central concept in quantum optics is the idea of the photon. The term “photon” was proposed in 1926 by Lewis [1] to denote a minimum portion of light energy instead of the term “quantum of light” proposed by Einstein [2].

As a result of the progress in quantum optics over the last few decades accompanied by the rapid proliferation of micro- and nanofabrication technologies, researchers are equipped with reliable methods for generation, manipulation, and characterization of single photons and combination of photons, especially correlated photon pairs. This fact stimulated the birth of quantum informatics – a new interdisciplinary branch of science and technology at the intersection of quantum physics, mathematics, and engineering, underlying new quantum methods of processing, storage, transmission, and protection of information [3–5].

Today, a number of single photon sources have been suggested and demonstrated based on different physical objects [6]. Among them are quantum dots [7, 8], single atoms [9] and ions [10], as well as NV-centers in diamonds [11].

The creation of generation techniques of correlated photon pairs, especially entangled ones, qualitatively changed the current status of quantum optics. It is difficult to overestimate the role of biphoton sources in the development of quantum cryptography [12, 13], quantum communication [4], quantum computing [14], and fundamental research [15].

The generation of biphoton quantum states has been demonstrated using a SPDC in bulk nonlinear crystals [16, 17] and in microstructured fibers [18], employing four-wave mixing in doped [19] and microstructured fibers [20, 21], in cold atom ensembles [22], as well as utilizing the two-photon emission in semiconductors [23]. For further details, see, for example, the review article [24].

In this paper, we provide a brief review of the methods for generation and applications of single photon and biphoton quantum states. In addition, we present an experimental study of SPDC-based source of time-correlated pairs of photons at 1,064 nm. Two configurations of the source have been investigated, namely, single-crystal configurations capable of producing separable photon pairs and double-crystal configurations used for generation of polarization-entangled photon pairs. The choice of a wavelength of 1,064 nm was motivated by a possible future application of such sources in cryptographic systems implemented in existing fiber-based networks along with retransmitters on Nd:YAG crystals. It should be noted that this wavelength was previously not widely used because of the rather low quantum efficiency of the detectors in this spectral region. However, recent progress in single-photon detection makes this spectral region more attractive. Also, we present the characteristics of the generated photon states using the quantum tomography approach. In addition, for the double-crystal configuration we describe the Migdall effect that caused degradation of the entanglement degree of generated quantum states.

2. SPDC Sources of Correlated Photon Pairs

Sources of photon pairs based on SPDC are among the most reliable sources of time-correlated photons. Moreover, they have relatively simple technical designs. Photon pairs emitted from such sources show a high degree of correlation in time and energy. Additionally, they can also be entangled in frequency, polarization, and angular momentum [25–27]. Currently, the SPDC-based sources of correlated entangled and separable photons have deservedly taken their rightful place in modern optical technologies.

The effect of spontaneous parametric scattering, which was first pointed out in 1966 by Klyshko [28, 29], has been immediately observed experimentally in three groups [30–32]. The first theoretical explanation of this effect was given in 1967–1968 [29, 33], followed by a number of theoretical studies of quantum properties of SPDC photon pairs [34–36]. Quantum properties of SPDC photons were first investigated experimentally in 1970 [37], where simultaneous generation of SPDC photons was first demonstrated. More sophisticated schemes such as, for example, the four-photon SPDC were also studied [38].

After the emergence of SPDC sources, much more opportunities were opened to physicists. With the help of these sources, a great number of experiments have been performed, which made a significant contribution to quantum optics and significantly advanced this new area of knowledge. This allowed one to manage the absolute calibration of photodetectors [39, 40] and to provide the possibility of weak signal communication below the noise level [41, 42]. These experiments were a great boost to the development of modern cryptography [5], which was first demonstrated experimentally in 1992 [43]. SPDC entangled photons have also played a significant role in the development of quantum computing and quantum information [3, 4], quantum teleportation [44, 45], as well as in elaborating the fundamental concepts of quantum optics. Fundamental quantum properties of photons [46–48], quantum cloning [49], entanglement, and quantum nonlocality [50–52], including the Bell theorem [53, 54], multiphoton entan-

glement [55–60], and single-photon Fock states [61], have been studied. Some interesting facts about the role of SPDC photons in the development of quantum optics can be found in [62, 63].

SPDC sources of photon pairs [64] have unique properties. Along with constructive simplicity, such sources generate photons with entanglement close to unity [65], having at the same time a large brightness [17]. Apart from this, there is a possibility to control the frequency and spatial characteristics of the SPDC biphoton field [66].

Phenomenologically, SPDC is the effect of the pump photon decay into two photons [29,30], called the signal (photon with a higher frequency) and the idler (photon with lower frequency), due to scattering by zero-point fluctuations of the vacuum in a quadratic nonlinear medium. The process requires meeting the so-called phase matching conditions:

$$\omega_p = \omega_s + \omega_i, \quad \vec{k}_p = \vec{k}_s + \vec{k}_i, \tag{1}$$

where $\omega_p, \omega_s, \omega_i$ and $\vec{k}_p, \vec{k}_s, \vec{k}_i$ are angular frequencies and wave vectors of pump, signal, and idler waves, respectively. The phase matching conditions (1) technically may be met in two ways [67] — using type-I [17] or type-II [16, 68] interactions.

Double-crystal sources of type-I can emit entangled photons in the polarization state

$$|\Psi_I\rangle = \frac{|HH\rangle + e^{i\delta}|VV\rangle}{\sqrt{2}}, \tag{2}$$

while type-II sources are capable of emitting photons in the polarization state

$$|\Psi_{II}\rangle = \frac{|HV\rangle + e^{i\delta}|VH\rangle}{\sqrt{2}}, \tag{3}$$

where $|H\rangle$ and $|V\rangle$ denote the horizontal and vertical polarization, respectively, and δ is the relative phase between the fields generated in the crystals.

Further, we will focus on type-I sources based on negative crystals. Usually noncollinear interaction is used in such sources because the photons of the pair are easier to separate over space (Fig. 1).

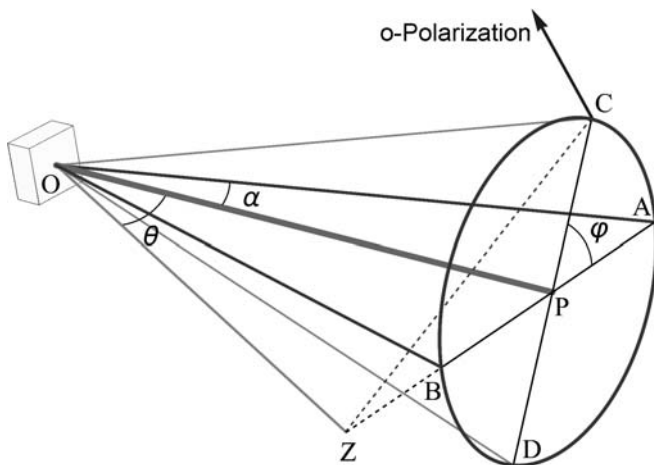


Fig. 1. Geometry of noncollinear parametric interaction under the conditions of type-I synchronism. The pump beam OP and the optical axis OZ form a horizontal plane. The plane OCZ is the principle plane of the scattering beam OC . The labeled components shown are the angle between the pump beam and the optic axis (θ) and the polar (φ) and azimuthal (α) angles of scattering. The o -polarization vector is normal to the principal plane OCZ and exhibits the wave polarization.

In the case of $e \rightarrow oo$ synchronism, the pump is the extraordinary polarized wave and the scattered waves are ordinary polarized. The ordinary wave polarization [67] is orthogonal to the principal scattering plane, which contains the optical axis of the crystal and the direction of propagation of scattered waves.

Usually the down-converted light is collected from the OA and OB directions, as shown in Fig. 1. This causes the scattered light to be vertically polarized.

Using a single-crystal scheme shown in Fig. 1, it is possible to obtain the time-correlated photons (even in the case of a cw pump) but the polarization-entangled photons cannot be produced by such a source. One of the most frequently used schemes for generation of polarization-entangled photon pairs is the double-crystal scheme proposed in [17].

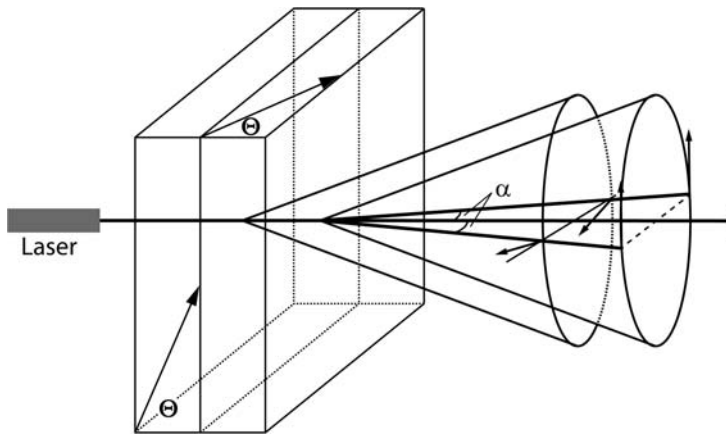


Fig. 2. Double-crystal scheme for generation of polarization-entangled photon pairs. Here, θ is the angle between the pump beam and the crystal axis, and α is the azimuthal angle of scattering. Polarization of scattered waves is denoted by arrows.

The scheme consists of two identical type-I nonlinear crystals that are orthogonally oriented and placed one after the other (Fig. 2). The pump beam, being polarized at 45° to the horizontal direction, splits in the crystals into ordinary and extraordinary polarized waves pumping the crystals. The scattered light generated in the crystals is spatially overlapped. If there is no way to identify (without polarization measurements) in which of the two crystals the photon pair is created, the generated fields are added coherently. In the first approximation, we can assume that the first crystal generates a field polarized along the horizontal direction $|H\rangle$, and the second crystal along the vertical direction $|V\rangle$. When the amplitudes of the biphoton fields are equal, the pair of crystals will generate the photon pairs in the state (2). The phase δ arises from the fact that the biphoton field begins to emerge in the first and second crystals with different phases determined by the phase of the pump and different phase shifts occurring during the passage of the pairs through the crystals. The phase δ can be controlled by changing the ellipticity of the pump polarization.

To produce the state (2) in the experiment, one should take into account the factors suppressing the purity and entanglement of the state. The most vigorous of them are the timing information (provided by the pump coherence time) and the spatial-mode-dependent phase (making the phase δ dependent on the scattering angle). The presence of both these factors can be successfully eliminated by placing specially designed compensation crystals into the scheme.* But there is one more factor that can reduce the entanglement in such sources due to deviation of the scattered light polarization depending on the angle of scattering, the so-called Migdall effect [70, 71]. We plan to publish a detailed analysis of the influence of polarization deviation in SPDC on entanglement in the nearest future. Here, we would like to pay attention only to a specific feature of the Migdall effect.

If the relative phase δ [see (2)] between the fields generated in the two crystals is equal to zero, the Migdall effect does not reduce the polarization entanglement in the double-crystal scheme. Indeed, let us consider the crystal geometry shown in Fig. 2. Polarizations of the waves generated in the first crystal

*For further details, see the original paper [69].

is subjected to the Migdall effect. In the second crystal, there are no polarization deviations at all. Polarization deviations for both scattered photons are equal in magnitude and opposite in sign. If we assume that $\delta = 0$, the symmetry of the process allows one to write the explicit form of the state [72]:

$$|\Psi\rangle = \frac{1}{\sqrt{2}} \left(|H\rangle \otimes \hat{S}(\beta)|H\rangle + |V\rangle \otimes \hat{S}(\beta)|V\rangle \right), \quad (4)$$

where β is the angle of the polarization rotation of the light generated in the first crystal due to the Migdall effect and

$$\hat{S}(\alpha) = \begin{pmatrix} \cos \alpha & -\sin \alpha \\ \sin \alpha & \cos \alpha \end{pmatrix} \quad (5)$$

is the rotation matrix acting in the one-qubit subspace.

It can be shown that the state (4) can be transformed to the Bell state by a few single-qubit operations, which means that this state is maximally entangled.

It is important to note that compensation techniques for elimination of entanglement suppression caused by the Migdall effect have not been proposed so far.

3. Source of Time-Correlated Photons at 1.064 μm

The developed source produces the time-correlated photons at a wavelength of 1.064 μm . It can operate in two modes: in the regime of generation of separable photons and in the regime of generation of polarization-entangled photons.

3.1. Generation of Separable Time-Correlated Photons

A setup for generation of separable photon pairs is shown in Fig. 3.

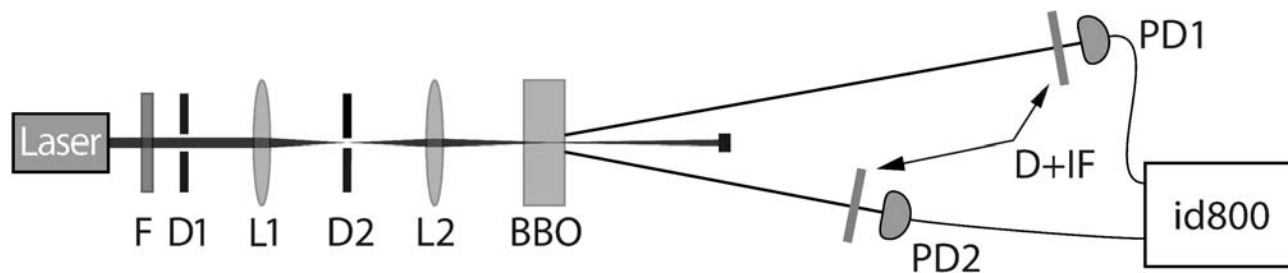


Fig. 3. Setup for generation of separable photons. The labeled components are iris diaphragms (D, D1, D2), collimating lenses (L1, L2), an SZS-21 spectral filter (F), ID Quantique id400 single-photon-counting detectors (PD1, PD2), Thorlabs FLH051064-8 interference filters (IF), and nonlinear crystal (BBO). Here, Id800 is the time-to-digital converter made by ID Quantique.

The pump laser is a frequency-doubled diode-pumped Nd:YAG cw ATC 53-350 laser. It has a central frequency of 532 ± 0.2 nm measured with a MDR-3 monochromator having a diffraction grating of 1,200 lines/mm. The pump laser has a coherence length of ~ 3 mm and a maximum power of ~ 350 mW. The laser operates at the TEM₀₀ mode with a diameter of ~ 0.5 mm and divergence of ~ 3 mrad. The angle beam stability is not worse than 0.2 mrad. The stability of the pump power during one hour is not

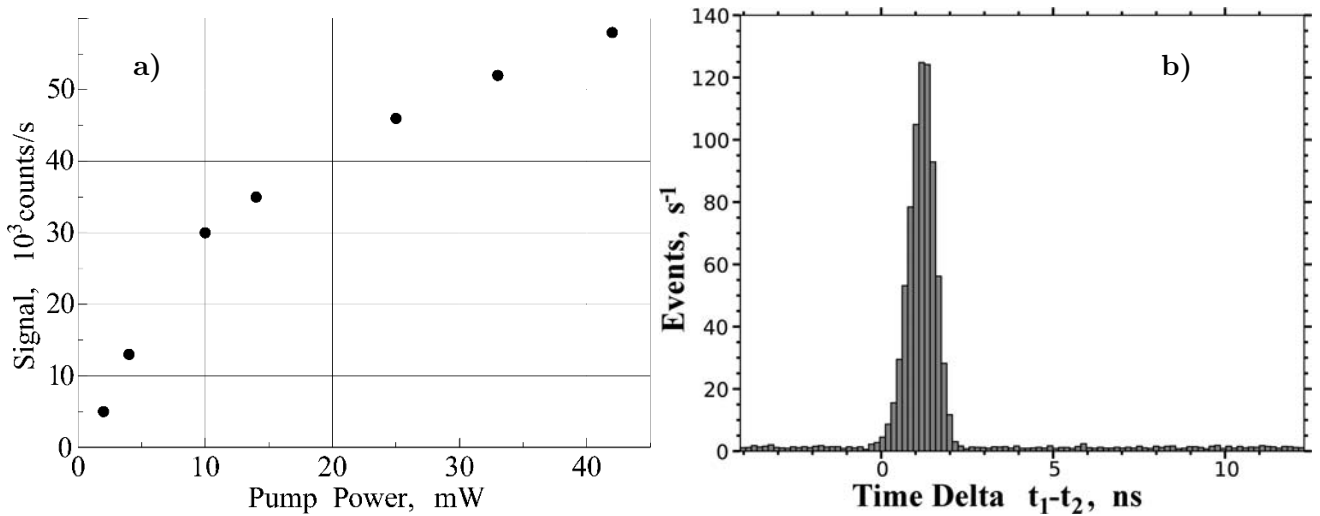


Fig. 4. Characteristics of the source operating in the regime of generation of separable time-correlated photons. Here, the dependence of the counting rate on the pump power (a) and the joint photon counting histogram in the absence of time delay between the measuring channels (b).

worse than 5%. The output polarization is tilted by 45° to the horizontal direction and is rotated to be horizontal. The polarization contrast is $\sim 100:1$.

A pump beam passes through a blocking filter F (an SZS-21 blue-green glass filter) cutting the residual radiation at $1.064 \mu\text{m}$. The collimator (lenses L1 and L2, diaphragms D1 and D2) provides a pump beam waist of ~ 1 mm inside the BBO crystal. The BBO crystal is a $5 \times 5 \times 3$ mm $\beta\text{-BaB}_2\text{O}_4$ crystal cut for frequency-degenerated type-I phase matching. The external half-opening angle is 3° . Scattered light, having a wavelength centered at $1.064 \mu\text{m}$, passes through iris diaphragms D and interference filters IF and is focused by objectives into PD (a $1.064 \mu\text{m}$ single-photon counter id400 produced by ID Quantique). The objectives transmit the image of the SPDC spot formed inside the BBO crystal to an active photodiode area with reduction $1:10$. The interference filter IF is a Thorlabs FLH051064-8 filter with a central wavelength of $1.064 \mu\text{m}$ and bandwidth of 8 nm FWHM. Output signals from the detectors are analyzed by a time-to-digital converter id800, also from ID Quantique.

The id400 avalanche photodetectors have a dead time of $\sim 10 \mu\text{s}$ and quantum efficiency of $\sim 30\%$. The id800 time-to-digital converter has a bin size of 81 ps.

The dependence of the counting rate on the pump power is shown in Fig. 4a. The graph shows that the source is able to operate reliably at relatively low pump levels of a few mW. For instance, at 10 mW the number of photon counts reaches 30,000 per second, which is already fairly close to the technical counting rate limit of the photodetectors (10^5 s^{-1}) defined by the detector dead time ($\sim 10 \mu\text{s}$).

The joint photon counting histogram in the absence of time delay between the photons in a pair is shown in Fig. 4b. The width of the distribution is approximately 1 ns. In principle, the width should display the spread of photons in time. However, it is known that photons must be correlated with a significantly shorter time spread [48]. So the obtained value 1 ns demonstrates the jitter of our apparatus, which turned out to be rather small.

In this configuration, the wave function of generated light can be expressed as

$$|\Psi_{vv}\rangle = |V\rangle \otimes |V\rangle, \quad (6)$$

i.e., the state is pure and separable and, hence, it is characterized by the von Neumann entropy and a

tangle equal to zero. The measurements carried out with the help of the quantum tomography system have confirmed the expectations.

3.2. Generation of Entangled Photons

A scheme of the source operating in the entangled-photon regime is shown in Fig. 5. The experimental setup may be divided into two parts: the SPDC source and the apparatus for quantum-state tomographic measurements.

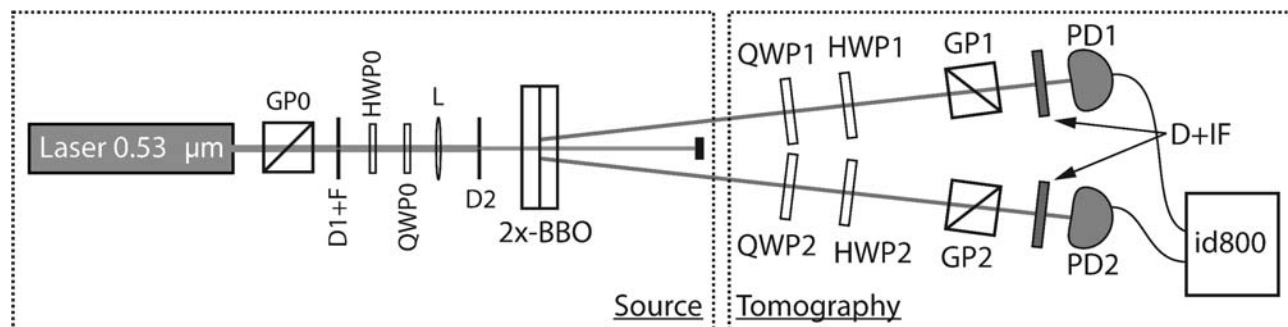


Fig. 5. Scheme of the source of entangled photons based on two BBO crystals. The labeled components are Glan prisms (GP0, GP1, GP2), half-wave plates (HWP0, HWP1, HWP2), quarter-wave plates (QWP0, QWP1, QWP2), and dual nonlinear crystal ($2x$ -BBO). The other notations are the same as those shown in Fig. 3.

The pump source is the same ATC 53-350 laser described above. The GP0 Glan prism increases the polarization contrast of the pump beam up to $\approx (10^4 - 10^5) : 1$. The HWP0 half-wave plate rotates the pump polarization by 45 degrees. The QWP0 quarter-wave plate can be tilted and attains the ellipticity of the pump polarization.

The collimation system is the same as in the regime of time-correlated separable photons. The crystals $2x$ -BBO are two β -BaB₂O₄ crystals cut in the same manner as the crystal in the previous scheme but having different sizes $5 \times 5 \times 0.5$ mm. The crystals are rotated orthogonally to each other. Orientations of the optical axes are shown in Fig. 2.

The source also has a filtering system consisting of the iris diaphragms (having diameter 5 – 7 mm) placed 1 m after the crystals. The IF Thorlabs FLH051064-8 interference filters are placed just in front of the objectives.

The quantum tomography system consists of the quarter-wave plates (QWP1, QWP2), half-wave plates (HWP1, HWP2), and Glan prisms (GP1, GP2) placed in each spatial mode. The scheme allows one to perform an arbitrary single-qubit polarization transform and projection in each mode separately. As in the previous scheme, the down-converted light was focused onto the ID Quantique id400 detectors, and the output signals were processed by an id800 time-to-digital converter.

3.3. Tomographic Measurements of the Polarization Photon-Pair State

The possibility of characterizing the quantum states of photons generated by the source is enormously important for quantum optics experiments. The main task of characterization is the measurement of quantum entanglement of generated photon pairs. Currently, the best way for exhaustive characterization of quantum states is quantum tomography.

The problem of estimating the quantum state in an ensemble was studied for the first time by Fano [73]. The heart of quantum tomography is the fact that with the help of a series of measurements on a large number of identical copies of a quantum system one can obtain full information on the quantum state. In particular, to determine the polarization state of the photon pair, this procedure requires 16 different measurements. Quantum tomography, originated in 1993 by Raymer [74], has become a powerful tool for quantitative characterization of the quantum state of entangled photons [75–80]. A detailed review of quantum tomography can be found in [81].

The quantum tomography procedure allows one to deduce the density matrix elements by measuring mean values of various observables, in contrast to the backwards problem of calculating the observables using the density matrix.

The set of observables (or measurements), which allows one to deduce all of the density matrix elements, is called the tomographically complete set of measurements. There are many such sets, so that their choice is a question of experimental convenience. We opted the set proposed in [82] requiring only one optical element (wave plate) to change its position between the tomographic measurements. The set of measurements is shown in Table 1.

Experimental results for polarization-entangled photon pairs are shown in Table 2 with experimental coincidence counting rates obtained for every measurement from the set listed in Table 1.

The likelihood approximation of the density matrix calculated from the above data is

$$\hat{\rho}_{\text{likelyhood}}^{\text{source}} = \begin{pmatrix} 0.8448 & 1.036 \cdot 10^{-2} + i3.764 \cdot 10^{-2} & 2.115 \cdot 10^{-2} + i8.827 \cdot 10^{-3} & 0.4711 - i7.049 \cdot 10^{-2} \\ 1.036 \cdot 10^{-2} - i3.764 \cdot 10^{-2} & 8.914 \cdot 10^{-3} & 4.753 \cdot 10^{-3} - i3.849 \cdot 10^{-3} & 1.681 \cdot 10^{-2} - i4.475 \cdot 10^{-2} \\ 2.115 \cdot 10^{-2} - i8.827 \cdot 10^{-3} & 4.753 \cdot 10^{-3} + i3.849 \cdot 10^{-3} & 4.344 \cdot 10^{-3} & 2.969 \cdot 10^{-2} - i1.076 \cdot 10^{-2} \\ 0.4711 + i7.049 \cdot 10^{-2} & 1.681 \cdot 10^{-2} + i4.475 \cdot 10^{-2} & 2.969 \cdot 10^{-2} + i1.076 \cdot 10^{-2} & 0.5023 \end{pmatrix}. \quad (7)$$

Table 1. Tomographically Complete Set [82] of Measurements.

n	Spatial mode 1	Spatial mode 2	h_1	q_1	h_2	q_2
1	$ H\rangle$	$ H\rangle$	45°	0°	45°	0°
2	$ H\rangle$	$ V\rangle$	45°	0°	0°	0°
3	$ V\rangle$	$ V\rangle$	0°	0°	0°	0°
4	$ V\rangle$	$ H\rangle$	0°	0°	45°	0°
5	$ R\rangle$	$ H\rangle$	22.5°	0°	45°	0°
6	$ R\rangle$	$ V\rangle$	22.5°	0°	0°	0°
7	$ D\rangle$	$ V\rangle$	22.5°	45°	0°	0°
8	$ D\rangle$	$ H\rangle$	22.5°	45°	45°	0°
9	$ D\rangle$	$ R\rangle$	22.5°	45°	22.5°	0°
10	$ D\rangle$	$ D\rangle$	22.5°	45°	22.5°	45°
11	$ R\rangle$	$ D\rangle$	22.5°	0°	22.5°	45°
12	$ H\rangle$	$ D\rangle$	45°	0°	22.5°	45°
13	$ V\rangle$	$ D\rangle$	0°	0°	22.5°	45°
14	$ V\rangle$	$ L\rangle$	0°	0°	22.5°	90°
15	$ H\rangle$	$ L\rangle$	45°	0°	22.5°	90°
16	$ R\rangle$	$ L\rangle$	22.5°	0°	22.5°	90°

Table 2. Number of Coincidence Counts in Various Tomographic Measurements with n , the Number of the Measurement from Table 1.

n	Coincidence counts						
1	12857	5	6597	9	6335	13	7402
2	234	6	5359	10	14108	14	6744
3	13153	7	7363	11	5820	15	5430
4	113	8	7002	12	6493	16	12045

This allowed us to deduce the purity and entanglement state characteristics [4,83–85]. Results are shown in Table 3.

From the density matrix (7), one can deduce its eigenvalues and eigenvectors. The higher-order eigenvalue turned out to be ~ 0.97 , i.e., this entangled state is generated by the source elaborated with the probability of $\sim 97\%$.

Table 3. Purity and Entanglement Characteristics of the State.

Variable	Value
von Neumann entropy	0.17 ± 0.05
Linear entropy	0.064 ± 0.028
Concurrence	0.945 ± 0.019
Tangle	0.894 ± 0.035
Entanglement of formation	0.922 ± 0.027

The corresponding eigenvector reads

$$|\Psi^{\text{src}}\rangle = \begin{pmatrix} -0.698 \\ -0.025 + 0.058i \\ -0.038 + 0.011i \\ -0.704 - 0.104i \end{pmatrix}; \quad (8)$$

this means that the generated state has fidelity, with the maximum entangled state (2) equal to

$$|\langle \Psi^{\text{src}} | \Psi_I \rangle|^2 \Big|_{\delta=0} \approx 99\%,$$

which shows a high degree of entanglement.

4. Summary

Along with a brief overview of the single and biphoton sources, we presented the source of time-correlated photons at $1.064 \mu\text{m}$ and the results of its characterization obtained using quantum tomography. As we mentioned in the Introduction, the sources with such a wavelength are compatible with the Nd:YAG laser active medium, which is one of the most reliable working laser media used now in modern laser technologies. In view of the low pump power required for such SPDC sources, it may be implemented as a single microblock composed of a semiconductor pump crystal, Nd:YAG crystal, a second harmonic crystal, and a pair of SPDC crystals; the total size and power are compared with the sources pumped by semiconductor lasers. However, the source elaborated has a clear advantage in the degree of spatial and temporal coherence.

The density matrix (7), purity, and entanglement characteristics along with the explicit form of the state were deduced from the tomographic measurements of biphotons generated by our source. We showed that the state generated has a fidelity corresponding to the Bell state of $\sim 99\%$ being generated with a probability of $\sim 98\%$.

The source elaborated was successfully applied to the quantum key distribution through the airspace on the basis of a specially developed time algorithm. Some results on the use of the source for this purpose can be found in [86].

It is worth noting that in our experiments along with a id800 ID Quantique time-to-digital converter we used a home-made time-to-digital converter TDC-6, which has similar characteristics and a significant cost advantage.

We also briefly touched upon the problem of entanglement suppression caused by the Migdall effect. The results obtained can be useful for future work directed to restricting the negative impact of the Migdall effect in a double-crystal SPDC scheme.

Acknowledgments

This study was financially supported by the Laboratory of Optoelectronic Devices Ltd. The authors thank Prof. A. Chirkin for fruitful discussions and Dr. N. Nagorskiy and D. Agapov and N. Gavrev, students of the M. V. Lomonosov Moscow State University, for their help in carrying out the work at different stages, as well as D. Yakovlev and M. Turaev for elaborating the TDC-6 device.

References

1. G. N. Lewis, *Nature*, **118**, 874 (1926).
2. A. Einstein, *Ann. Phys.*, **17**, 132 (1905).
3. M. A. Nielsen and I. L. Chuang, *Quantum Computation and Quantum Information*, Cambridge University Press (2000).
4. D. Bouwmeester, A. Ekert, and A. Zeilinger, *The Physics of Quantum Information*, Springer, Berlin (2000).
5. H. K. Lo, M. Curty, and K. Tamaki, *Nature Photon.*, **8**, 595 (2014).
6. S. Takeuchi, *Jpn J. Appl. Phys.*, **53**, 030101 (2014).
7. P. Michler, A. Kiraz, C. Becher, et al., *Science*, **290**, 2282 (2000).
8. A. Dousse, J. Suffczynski, A. Beveratos, et al., *Nature*, **466**, 217 (2010).
9. A. Kuhn, M. Hennrich, and G. Rempe, *Phys. Rev. Lett.*, **89**, 067901 (2002).
10. M. Keller, B. Lange, K. Hayasaka, et al., *Nature*, **431**, 1075 (2004).
11. R. Albrecht, A. Bommer, C. Pauly, et al., *Appl. Phys. Lett.*, **105**, 073113 (2014).
12. C. H. Bennett and G. Brassard, *Quantum Cryptography: Public Key Distribution and Coin Tossing, Proceedings of IEEE ICC, Systems and Signal Processing (Bangalore, 1984)*.
13. S. Pirandola, C. Ottaviani, G. Spedalieri, et al., *Nature Photon.*, **9**, 397 (2015).
14. R. Raussendorf and H. J. Briegel, *Phys. Rev. Lett.*, **86**, 5188 (2001).
15. A. Zeilinger, G. Weihs, T. Jennewein, and M. Aspelmeyer, *Nature*, **433**, 230 (2005).
16. P. G. Kwiat, K. Mattle, H. Weinfurter, et al., *Phys. Rev. Lett.*, **75**, 4337 (1995).
17. P. G. Kwiat, E. Waks, A. G. White, et al., *Phys. Rev. A*, **60**, R773 (1999).
18. A. B. U'Ren, C. Silberhorn, K. Banaszek, and I. A. Walmsley, *Phys. Rev. Lett.*, **93**, 093601 (2004).
19. J. E. Sharping, K. F. Lee, M. A. Foster, et al., *Opt. Exp.*, **14**, 12388 (2006).
20. O. Alibart, J. Fulconis, G. K. L. Wong, et al., *New J. Phys.*, **8**, 67 (2006).
21. J. Fan, A. Dogariu, and L. J. Wang, *Opt. Lett.*, **30**, 1530 (2005).
22. L. Xiao-Song, C. Qun-Feng, S. Bao-Sen, and G. Guang-Can, *Chin. Phys. Lett.*, **26**, 064204 (2009).
23. A. Hayat, P. Ginzburg, and M. Orenstein, *Nature Photon.*, **2**, 238 (2008).
24. M. D. Eisaman, J. Fan, A. Migdall, and S. V. Polyakov, *Rev. Sci. Instrum.*, **82**, 071101 (2011).
25. G. Milione, S. Evans, D.A. Nolan, and R.R. Alfano, *Phys. Rev. Lett.*, **108**, 190401 (2012).
26. F. Cardano, E. Karimi, S. Slussarenko, et al., *Appl. Opt.*, **51**, C1 (2012).
27. A. Vaziri, G. Weihs, and A. Zeilinger, *Phys. Rev. Lett.*, **89**, 240401 (2002).
28. D. N. Klyshko, Talk at the All-Union Workshop on Nonlinear Properties of Media (Chernogolovka, Moscow Region, 1966).
29. D. N. Klyshko, *JETP Lett.*, **6**, 23 (1967).
30. S. A. Akhmanov, V. V. Fadeev, R. V. Khokhlov, and O. N. Chunaev, *JETP Lett.*, **6**, 575 (1967).
31. S. E. Harris, M. K. Oshman, and R. L. Byer, *Phys. Rev. Lett.*, **18**, 732 (1967).

32. M. Douglas and H. Mahr, *Phys. Rev. Lett.*, **18**, 905 (1967).
33. T. G. Giallorenzi and C. L. Tang, *Phys. Rev.*, **166**, 225 (1968).
34. B. R. Mollow, *Phys. Rev. A*, **8**, 2684 (1973).
35. C. K. Hong and L. Mandel, *Phys. Rev. A*, **31**, 2409 (1985).
36. A. Joobeur, B. E. A. Saleh, and M. C. Teich, *Phys. Rev. A*, **50**, 3349 (1994).
37. D. C. Burnham and D. L. Weinberg, *Phys. Rev. Lett.*, **25**, 84 (1970).
38. S. M. Arakelian, V. G. Tunkin, A. I. Kholodnykh, and A. S. Chirkin, *Zh. Tekh. Fiz.*, **44**, 1253 (1974).
39. D. N. Klyshko, *Sov. J. Quantum Electron.*, **10**, 1112 (1980).
40. A. A. Malygin, A. N. Penin, and A. V. Sergienko, *JETP Lett.*, **33**, 477 (1981).
41. L. Mandel, *J. Opt. Soc. Am. B*, **1**, 108 (1984).
42. C. K. Hong, S. R. Friberg, and L. Mandel, *Appl. Opt.*, **24**, 3877 (1985).
43. C. H. Bennett, F. Bessette, G. Brassard, et al., *J. Cryptol.*, **5**, 3 (1992).
44. D. Bouwmeester, J. W. Pan, K. Mattle, et al., *Nature*, **390**, 575 (1997).
45. M. Yu. Saygin, A. S. Chirkin, and M. I. Kolobov, *J. Opt. Soc. Am. B*, **29**, 2090 (2012).
46. P. Grangier, G. Roger, and A. Aspect, *Europ. Phys. Lett.*, **1**, 173 (1986).
47. C. K. Hong and L. Mandel, *Phys. Rev. Lett.*, **56**, 58 (1986).
48. C. K. Hong, Z. Y. Ou, and L. Mandel, *Phys. Rev. Lett.*, **59**, 2044 (1987).
49. D. Pelliccia, V. Schettini, F. Sciarrino, et al., *Phys. Rev. A*, **68**, 042306 (2003).
50. Y. H. Shih and C. O. Alley, *Phys. Rev. Lett.*, **61**, 2921 (1988).
51. J. W. Pan, D. Bouwmeester, H. Weinfurter, and A. Zeilinger, *Phys. Rev. Lett.*, **80**, 3891 (1998).
52. L. Hardy, *Phys. Rev. Lett.*, **71**, 1665 (1993).
53. Z. Y. Ou and L. Mandel, *Phys. Rev. Lett.*, **61**, 50 (1988).
54. D. M. Greenberger, M. A. Horne, A. Shimony, and A. Zeilinger, *Am. J. Phys.*, **58**, 1131 (1990).
55. D. Bouwmeester, J. W. Pan, M. Daniell, et al., *Phys. Rev. Lett.*, **82**, 1345 (1999).
56. J. W. Pan, D. Bouwmeester, M. Daniell, et al., *Nature*, **403**, 515 (2000).
57. Z. Zhao, Y. A. Chen, A. N. Zhang, et al., *Nature*, **430**, 54 (2004).
58. C. Y. Lu, X. Q. Zhou, O. Gühne, et al., *Nature Phys.*, **3**, 91 (2007).
59. W. B. Gao, C. Y. Lu, X. C. Yao, et al., *Nature Phys.*, **6**, 331 (2010).
60. X. C. Yao, T. X. Wang, P. Xu, et al., *Nature Photon.*, **6**, 225 (2012).
61. A. I. Lvovsky, H. Hansen, T. Aichele, et al., *Phys. Rev. Lett.*, **87**, 050402 (2001).
62. G. Greenstein and A. Zajonc, *The Quantum Challenge: Modern Research on the Foundations of Quantum Mechanics*, Jones & Bartlett Learning, Sudbury, MA (2006).
63. A. Zeilinger, *Dance of the Photons: From Einstein to Quantum Teleportation*, Macmillan (2010).
64. K. Edamatsu, *Jpn J. Appl. Phys.*, **46**, 7175 (2007).
65. R. Rangarajan, M. Goggin, and P. Kwiat, *Opt. Exp.*, **17**, 18920 (2009).
66. L. E. Vicent, A. B. U'Ren, R. Rangarajan, et al., *New J. Phys.*, **12**, 093027 (2010).
67. V. G. Dmitriev, G. G. Gurzadyan, D. N. Nikogosyan, *Handbook of Nonlinear Optical Crystals*, Springer, Berlin (2013).
68. T. Kim, M. Fiorentino and F. N. C. Wong, *Phys. Rev. A*, **73**, 012316 (2006).
69. J. B. Altepeter, E. R. Jeffrey, and P. G. Kwiat, *Opt. Exp.*, **13**, 8951 (2005).
70. A. Migdall, *J. Opt. Soc. Am. B*, **14**, 1093 (1997).
71. R. Rangarajan, A. B. U'Ren, and P. G. Kwiat, *J. Mod. Opt.*, **58**, 312 (2011).
72. S. A. Magnitskiy, P. P. Gostev, D. N. Frolovstev, and V. V. Firsov, *Moscow Univ. Phys. Bull.*, **5**,

- 53 (2015).
73. U. Fano, *Rev. Mod. Phys.*, **29**, 74 (1957).
 74. D. T. Smithey, M. Beck, J. Cooper, and M. G. Raymer, *Phys. Rev. A*, **48**, 3159 (1993).
 75. G. M. D'Ariano, M. De Laurentis, M. G. A. Paris, et al., *J. Opt. B*, **4**, S127 (2002).
 76. J. L. O'Brien, G. J. Pryde, A. G. White, et al., *Nature*, **426**, 264 (2003).
 77. P. Walther, K. J. Resch, T. Rudolph, et al., *Nature*, **434**, 169 (2005).
 78. R. M. Stevenson, R. J. Young, P. Atkinson, et al., *Nature*, **439**, 179 (2006).
 79. S. S. Straupe, D. P. Ivanov, A. A. Kalinkin, et al., *Phys. Rev. A*, **87**, 042109 (2013).
 80. K. S. Kravtsov, S. S. Straupe, I. V. Radchenko, et al., *Phys. Rev. A*, **87**, 062122 (2013).
 81. G. M. D'Ariano, M. G. Paris, and M. F. Sacchi, *Quantum Tomography, Adv. Imaging Electron. Phys.*, **128**, 206 (2003).
 82. D. F. V. James, P. G. Kwiat, W. J. Munro, and A. G. White, *Phys. Rev. A*, **64**, 052312 (2001).
 83. R. Jozsa, *J. Mod. Opt.*, **41**, 2315 (1994).
 84. W. K. Wootters, *Phys. Rev. Lett.*, **80**, 2245 (1998).
 85. N. A. Peters, T. C. Wei, and P. G. Kwiat, *Phys. Rev. A*, **70**, 052309 (2004).
 86. P. P. Gostev, S. A. Magnitsky, N. M. Nagorsky, et al., *EPJ Web Conf.*, **103**, 10010 (2015).